Accepted Manuscript

Three-dimensional fault meshes and multi-layer shear in mass-transport blocks: Implications for fluid flow on continental margins

Davide Gamboa, Tiago M. Alves

Please cite this article as: Gamboa, Davide, Alves, Tiago M., Three-dimensional fault meshes and multi-layer shear in mass-transport blocks: Implications for fluid flow on continental margins, *Tectonophysics* (2015), doi: 10.1016/j.tecto.2015.02.007
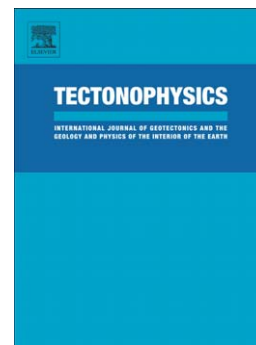
Three-dimensional fault meshes and multi-layer shear in mass-transport blocks: Implications for fluid flow on continental margins

Davide Gamboa*, Tiago M. Alves

3D Seismic Lab, School of Earth and Ocean Sciences, Cardiff University, Main Building,

Park Place, Cardiff, CF10 2FQ, United Kingdom

*Corresponding author: GamboaDA1@cf.ac.uk

Abstract

Submarine mass-transport deposits (MTDs) frequently include blocks of strata with variable deformation styles. In this paper, a 3D seismic volume from SE Brazil is compared with outcrop information from SE Crete to investigate multi-scale deformation patterns within mass-transport blocks. Block morphology relates closely to the orientation of internal faults and fractures, with wide chasms separating block fragments that opened along these planar features. Two families of sub-perpendicular faults associated with intra-block extension are observed on both scales. On seismic data, we show new evidence of intra-block horizontal shear and thrust faulting. At outcrop, downslope verging folds, load casts and injectites are observed along poorly consolidated sand-prone beds that are less than 1 m thick. Documented orientations and cross-cutting geometries suggest a syn-kinematic origin for these structures. By integrating the observations made at different scales we suggest the development of 3D meshes in MTD blocks, which are characterised by the intersection of faults and fractures with bed-parallel shear planes. These meshes greatly increase the relative permeability of individual blocks. The results in this work have implications for the analysis of fluid flow

paths on continental margins, and show that mass-transport blocks can comprise important fluid bypass points when buried in low permeability strata.

1. Introduction

Submarine Mass-Transport Deposits (MTDs) occur on continental margins worldwide, and reflect major sediment remobilization processes in deep marine settings (Hampton et al., 1996; Masson et al., 2006; Mulder and Cochonat, 1996; Posamentier, 2004). In these areas, slope failure is triggered when downslope-oriented shear stress exceeds the shear strength of weaker stratigraphic intervals (Hampton et al., 1996; Kvalstad et al., 2005; Nemec, 1990). Intense shear deformation is recorded in basal glide planes, which accommodate the bulk of the MTD movement (Alsop and Marco, 2013; Bull et al., 2009; Gee et al., 2005; Hampton et al., 1996). Above these same glide planes, distinct degrees of disaggregation are observed in MTDs depending on their remobilisation distance and original lithology (Bull et al., 2009; Callot et al., 2008; Gamboa et al., 2011; Lucente and Pini, 2008; Masson et al., 2006; Nemec, 1990). Thus, the incomplete disaggregation of MTDs is reflected by the presence of undeformed (or poorly deformed) strata, which later induce 3D permeability variations in buried successions (Alves et al., 2014; Beaubouef and Abreu, 2010; Gamboa et al., 2011; Posamentier and Martinsen, 2011; Weimer and Shipp, 2004). Often regarded as effective lateral and vertical barriers to fluid migration in sedimentary basins , the identification of sand and silt-prone MTDs on several continental margins has shown that such deposits can, instead, trap significant volumes of fluids (Alves et al., 2014; Ogiesoba and Hammes, 2012; Posamentier and Martinsen, 2011; Weimer and Shipp, 2004).

Heterogeneous MTDs in submarine and fossil landslides can include large (semi-) preserved fragments of strata, or mass-transport blocks (Alves and Lourenço, 2010; Bull et al., 2009; Callot et al., 2008; Dunlap et al., 2010; Dykstra et al., 2011; Gamboa et al., 2011; Gamboa et al., 2012; Ogata

2

et al., 2012). In this case, blocks can be classified as *remnant* or *rafted* depending on their degree of remobilisation. Remnant blocks comprise isolated *in situ* volumes of pre-failure strata that are not removed during the mass-transport event. Such blocks show a degree of stratigraphic continuity with underlying units and can be fault bounded (Alves, 2010; Bull et al., 2009; Frey-Martinez et al., 2005; Gamboa et al., 2011). In contrast, rafted blocks show variable degrees of remobilization, gliding sub-horizontally, rotating during downslope movement within, or glide beyond the toe the toe of MTDs (Bull et al., 2009; Ilstad et al., 2004; Kvalstad et al., 2005; Solheim et al., 2005). As with MTDs, rafted blocks record an increase in internal faulting and disaggregation with traveling distance, a character that results in the accumulation of progressively smaller blocks towards their distal accumulation zones (Bull et al., 2009; De Blasio et al., 2006; Jackson, 2011; Omosanya and Alves, 2013b).

Vertical faults and fractures are common in rafted and *in situ* mass-transport blocks (e.g. (Alves and Lourenço, 2010; Gamboa et al., 2011; Jackson, 2011). They usually accompany extensional and compressional structures at basal glide planes, in their ductile matrix, or in individual blocks (Bull et al., 2009; Dykstra et al., 2011; Frey-Martínez et al., 2006; Meckel III, 2011; Ogata et al., 2014; Ogata et al., 2012). Yet, deformation resulting from internal shear has not been documented in mass-transport blocks at seismic scales. Similarly, few examples of internal shear structures have been documented at outcrop, despite their importance as kinematic indicators and proxies for the understanding of physical processes in slope instability events (Ogata et al., 2012). In this study, the occurrence of multi-scale horizontal shearing is investigated within mass-transport blocks interpreted on a high-quality 3D seismic volume from SE Brazil, and outcropping carbonate blocks from SE Crete (Figs 1 and 2). Outcrop data is used in this paper as an analogue for structures identified on seismic data. We followed this approach with the aim of: 1) investigating scale-invariant deformation styles in remnant and rafted blocks, and 2) assessing the presence of fault and fracture meshes *sensu* Sibson (1996) within mass-transport blocks. Our results reveal that fault meshes interact with internal shear surfaces in individual blocks to enhance their relative

permeability. The data in this paper strengthens the premise that preferential permeable pathways exist within MTD blocks, a postulate with strong implications for the assessment of fluid migration on continental margins.

2. Data and methods

The interpreted 3D seismic volume covers an area of 2450 km^2 offshore Espírito Santo (Fig. 1a). Within this volume we selected a sub-area on the continental slope with multiple mass-transport blocks (Fig. 2a to 2c). The seismic volume has a SEG positive polarity, an inline spacing of 12.5 m and was acquired with a 6×5700 m array of streamers, processed to a 12.5 m×25 m bin grid. Data were sampled in intervals of 2 ms, for a nominal fold of 56. Data processing included resampling, amplitude recovery, time variant filtering, and predictive deconvolutions, prior to stacking and 3D pre-stack time migration using the full Kirchoff algorithm.

The interpretation of key seismic horizons on Petrel$^®$ was complemented by root-mean-square (RMS) amplitude maps and variance slices. RMS amplitude attribute highlights the average squared amplitude values from individual amplitude samples within a defined interval (Brown, 2004). Variance attributes convert a seismic volume of continuity (normal reflections) into a volume of discontinuity, highlighting faults and stratigraphic limits (Brown, 2004). Time-depth conversions used an estimated seismic velocity of 1800 m/s TWTT based on data from DSDP 515 (Barker et al., 1983). This value was used for to depth-convert faults and surfaces mapped on the seismic volume prior to to their analysis on 3D Stress$^®$. By estimating a mean frequency of 38 Hz within the stratigraphic interval of interest, we calculated a vertical resolution of 11.75 m within the blocks, i.e. equivalent to ¼ of an estimated wavelength of 47.3 m. The horizontal resolution is related to the Fresnel Zone, which on migrated 3D seismic data is reduced to a circle with a diameter of ¼ of a wavelength (Brown, 2004). Thus, the Fresnel zona of the seismic volume approaches 11.75 m in an horizontal direction at the depth in which mass-transport blocks are interpreted.

Outcrop data were acquired on the paleocontinental slope NW of Ierapetra, SE Crete (Fig. 1b). We collected sedimentological, structural, and photographic data of exposed carbonate blocks and slumps with the aim of documenting the local deformation styles. Paleostresses associated with faulting in mass-transport blocks were calculated based on the stress inversion method of McFarland et al. (2012). In this method, fault slip occurs when the shear stress equals or exceeds the normal stress acting on a fault surface (Lisle and Srivastava, 2004; Morris et al., 1996). The tendency of a fault to slip is thus defined as the ratio of normal to shear stress acting on a surface, depeding on its orientation and on the stress field (Morris et al., 1996). Slip tendency values allow the assessment of the likelihood and direction of slip on the fault surface analysed, and can be used as proxies for fault displacement (McFarland et al., 2012). In parallel, stress inversions evaluate the quality of stress tensors based on the degree of agreement between the slip tendency values and corresponding displacement values measured for a set of surfaces. Stress inversion is, therefore, the process of finding the stress state that optimizes this measure of agreement, with the inverted stress tensor being the one that best fits the fault displacement data (McFarland et al., 2012).

3. Geological setting

3.1. Espírito Santo Basin, SE Brazil

The Late Cretaceous and Cenozoic evolutions of the Espírito Santo Basin (ESB), SE Brazil, record two distinct tectonic phases (Fiduk et al., 2004; Ojeda, 1982). The late Aptian transitional phase records the deposition of thick evaporitic units in a restricted basin (Davison, 2007; Fiduk et al., 2004; Mohriak, 2003). Late Cretaceous to Cenozoic open marine sequences later draped the Aptian evaporites during the main opening stage of the Southern Atlantic Ocean (drift phase). In more detail, the early drift phase is characterised by a marine transgressive megasequence in which an Albian shallow-water carbonate platform was developed (Demercian et al., 1993; França et al., 2007). This carbonate platform was covered by Late Cretaceous-Paleocene mudstones deposited during a phase of deepening of the basin (Davison, 2007; Mohriak, 2003). The transition to the late

drift stage, during the Lower Eocene, marks the onset of a marine regressive megasequence and the development of a prograding slope fed from hinterland sources to the west, and from the Abrolhos Bank (Fig. 1a) (Fiduk et al., 2004; Mohriak, 2003, 2005).

Thin-skinned extension predominates in proximal areas of the ESB, where thin evaporites and salt welds connect pre- and post-salt units (Alves, 2012; Fiduk et al., 2004; França et al., 2007). This setting is followed by a region of developed diapirs on the mid-slope, and allochthonous salt walls and canopies in distal slope regions, where thick evaporites are present (Davison, 2007; Demercian et al., 1993; Fiduk et al., 2004; Mohriak et al., 1995). In such a setting, multiple Cenozoic mass-wasting events occurred in the ESB in association with regressive and transgressive cycles (Moreira and Carminatti, 2004), slope progradation and salt tectonics (Gamboa et al., 2011; Gamboa et al., 2010; Omosanya and Alves, 2013a, 2014). These cycles resulted in two major periods of slope instability in the study area of Mid-Eocene/Oligocene and Miocene age (Alves, 2010; Gamboa et al., 2010). In this work we focus on the deformation styles of blocks translated as part of an MTD accumulated on the proximal slope of the Espírito Santo Basin during the Miocene (Fig. 2b and 2c).

3.2. Ierapetra Basin, SE Crete

The Neogene geology of Crete is marked by alternating episodes of compressional and extensional tectonics that were associated to the southward migration of the Ionian trench system (Postma and Drinia, 1993). The paleoslope studied in this paper is located in SE Crete (Fig. 1b), and is located on the western flank of a half-graben (Ierapetra basin) formed during the Late Miocene (Fig. 2d). The Ierapetra basin is filled by Serravalian to Quarternary sediments that are up to 1000 m thick (Postma and Drinia, 1993). At the base of this succession is the Males Formation, an Upper Serravalian alluvial unit that gradually becomes marine towards its top. Lower Tortonian limestone-rich breccia conglomerates and mass-transport blocks of the Prina Series overlie the Males Formation (Postma and Drinia, 1993). The Prina Series is divided into a basal breccia series, and a

stratified series at its top (Postma and Drinia, 1993). A pronounced deepening event followed the deposition of the Prina Series, as recorded by the grey-blue (marine) marls and sands of the Kalamavka Formation. These marls and sands are covered by Tortonian deep-marine turbidites, marls and clays of the Makrilia Formation (Alves and Lourenço, 2010; Postma and Drinia, 1993). Late Tortonian tectonics in the Ierapetra Basin is marked by the fragmentation of breccia conglomerates (Prina Series) over Kalamavka and Makrilia marine deposits. This setting resulted in the sliding of mass-transport blocks on paleoslopes bounding the Ierapetra basin to the east and west (Alves and Lourenço, 2010; Postma and Drinia, 1993). These paleoslopes are now exposed due to tectonic uplift, which affected the island of Crete since the mid-Pliocene (Postma and Drinia, 1993).

4. The seismic-scale blocks in the Espírito Santo Basin

The deformation styles of a representative mass-transport block in the ESB were studied in detail using seismic and 3D fault modelling (Fig. 2 and 3). The studied block (Block A) is the largest of a Miocene MTD. It shows a maximum height of 350 m and an area of 13 Km^2 (Fig. 2b and 2c), and its long and short axis measure 4600 m and 3800 m, respectively. The base of Block A is paraconformable, whereas its top is irregular. Seismic data reveals distinct seismic facies, or sections, in Block A. These seismic sections are bounded by the negative high-amplitude Horizon 1, or H1 (Fig. 3). High-amplitude reflections predominate in the lower section (LS), while moderate amplitude reflections characterize the upper section (US) of Block A (Fig. 3).

Two main fault families occur in Block A, a WNW-ESE fault family and a NNE-SSW family (Figs. 3, 4 and 5). These faults are also identified on variance and RMS amplitude maps (Fig. 5). The NNE-SSW family includes a high number of faults with normal and reverse offsets (Fig. 5 and 6). The upper section of Block A shows smaller faults than the lower section. Large faults propagate through the full height of the block, at places bounding two main chasms (Fig. 3 and 6). Chasms Ch1 and Ch2 are up to 500 m in width, and follow a WNW-SE orientation (Fig 3, 5 and 6). The

7

chasms partially or fully segment the block along its vertical extent, causing any bounding faults to extend down to the basal surface of the MTD (Fig. 3b). Chasm width is either constant (Ch2) or shows a gradual increase (Ch1) with distance. In the latter case, the width of Ch1 gradually decreases from the western edge of the block towards its centre, accompanying an eastward decrease in block deformation and chasm height (Fig. 4a).

In Figure 3a is shown a seismic section striking parallel to the direction of transport of Block A. The figure highlights the presence of a frontal thrust anticline in the lower section of the block, and two faults and thrust anticlines in the upper section. These features indicate local compression in Block A. Thrust anticlines in the upper section are 1000 m apart and striking N030, verging towards the direction of movement of the MTD (Fig. 2c, 5e). Therefore, the strike of thrust faults and anticlines, and their SE vergence, provide a reliable kinematic indicator of the direction of movement of Block A.

Thrust faults observed towards the top of the block hint at the presence of a detachment surface along H1 (Fig. 3a). This same detachment coincides with a negative seismic reflection of lower impedance when compared with adjacent strata, a character often observed in sheared basal glide planes of MTDs (Ogata et al., 2014). The amplitude character of H1 suggests the presence of a soft, ductile interval at this level. RMS amplitude maps extracted within a 40 ms time window centred in H1 show a heterogeneous distribution of high amplitudes (Fig. 4b). Given their shape and orientation, these high-amplitude features can represent underconsolidated strata associated with slope turbidites preserved within Block A. Cenozoic and modern turbidite systems within the studied area of the Espírito Santo Basin show a predominant E to SE direction of flow (Fig. 2), identical to the orientation of the elongated high-amplitude features observed on RMS amplitude data (Fig. 4). We suggest that Block A preserved a fragment of the pre-failure slope, similarly to mass-transport blocks offshore Morocco (Dunlap et al., 2010). Alternatively, elongated high-amplitude features in H1 can indicate bed-parallel shear along this level (Fig. 4b).

Deformation styles in Block A suggest the presence of a complex stress distribution during its downslope movement, as revealed by the presence of extensional and compressional faults in close proximity (Fig. 3a and 6). Published models for mass-transport blocks imply an initial maximum direction of extension (σ_3) to be sub-parallel to the main direction of block remobilisation (Hampton et al., 1996; Kvalstad et al., 2005). Considering the strikes of faults observed in Block A and its direction of movement, one should would expect the predominance of a sub-horizontal minimum stress (σ_3) striking N120, and a sub-vertical maximum stress tensor (σ_1). In order to assess if these stress orientations are representative of the deformation styles observed in Block A, we modelled paleostress conditions in all mapped faults using 3D Stress®. Stress inversions for faults in Block A indicate paleostress conditions similar to the initially expected, with a SSE-oriented σ_3 plunging 22° along a N160 azimuth (Fig. 7a). The orientation of σ_1 also approaches the vertical, dipping circa 60° (Fig. 7a). However, the computed stress orientations do not correlate with the strikes of all mapped faults, particularly when considering individual thrust faults and their associated anticlines. To address this caveat, paleostress estimates were completed for specific fault types in Block A. Faults in the lower section, underneath H1, indicate paleostress conditions in which a SE minimum stress (σ_3) predominates (Fig. 7b). In contrast, faults in the upper section are more numerous and show two conjugate orientations. Stress inversions applied on NNE-SSW faults suggest an ESE-striking minimum stress (σ_3) with a N103 azimuth and 15° dip above H1 (Fig. 7c). In contrast, conjugate ESE-WNW faults relate to a N-S direction for σ_3 (Fig. 7d). In both cases σ_1 is sub-vertical and dips of 51° and 64°, respectively (Fig. 7c and 7d). Stress inversion data for thrust faults suggest a sub-horizontal σ_1 striking N110, being markedly different from the paleostress trends computed for normal faults, in which the maximum stress (σ_1) is sub-vertical (Fig. 7f).

The fit of paleostress tensors modelled on 3DStress® was assessed by analysing slip tendency values for all mapped faults and main shear surfaces (Fig. 8). Using paleostress conditions calculated for all faults (Fig. 7a), we observe that the majority shows slip tendencies between 0.4 and 0.6 (Fig. 8a). The main exceptions are chasm-bounding faults, which show a relatively low slip

tendency under the computed stress regime, although high slip is observed in one of the main faults bounding Ch1 (Fig. 8a). The lowest slip tendency values are observed along H1, but such scenario does not satisfactorily correlate with the sub-horizontal motions expected either at the basal glide plane, or at H1 level where thrust faults detach. However, conditions are met when the slip tendencies of the faults and surfaces are modelled with the paleostress results obtained from thrust fault inversions (Fig. 7f and 8b).

5. Outcrop-scale blocks: Ierapetra basin

In the Ierapetra Basin, outcropping mass-transport blocks vary in size and exhibit identical deformation styles (Figs. 9 and 10). Mass-transport blocks in the Males Formation do not exceed 4 m in height and have (exposed) widths between 2 m and 10 m. They are included in disaggregated strata, essentially comprising siliciclastic material and minor volumes of carbonate breccias (Fig. 9). Blocks in the Males Formation have rounded shapes, and are composed of sand alternating with gravelly beds that do not exceed 0.5 m in thickness (Fig. 9). These gravel beds are irregular and lense-shaped. Deformation styles in exposed blocks are related to lithological variations. Vertical fractures in cemented sand beds either terminate at the interface with unconsolidated gravelly beds, or are laterally offset by these (Fig. 9). In addition, horizontal offsets in cemented sand beds occur along gravel beds which present irregular thickness and pinch-and-swell structures (Fig. 9). We interpret these latter structures to derive from shearing along the gravelly beds during downslope movement of blocks.

Mass-transport blocks within the Prina Series are over 60 m in exposed height, frequently exceeding 200 m in length (Fig. 10). On the Ierapetra paleoslope, block movement followed an E-SE orientation over basal glide planes in the Males and Kalamavka Formations (Alves and Lourenço, 2010). Individual blocks are composed of up to 3 m thick beds of blue-grey carbonate breccias. Fine-grained sandstones occur in beds less than 1 m thick. Blocks show two main families of near-vertical fractures (Fig. 10 and 11). The principal family trends approximately N80 to N90,

sub-parallel to the long axis of blocks, and to downslope transport direction (Fig. 2d). A secondary family follows a NE-SW trend (N30 to N40) deforming the mass-transport blocks along their width. Blocks commonly show well-defined quadrangular to rectangular shapes, with linear frontal and lateral flanks sub-parallel to the two interpreted fracture orientations (Fig. 10). Chasms show orientations consistent with the strike of documented fault and fracture families, as also observed in SE Brazil (Fig. 2c and 10). Stress inversion of the E-W faults and fractures observed at outcrop suggest paleostresses with a sub-horizontal minimum stress (σ_3) striking N157, consistent with main direction of block movement, and sub-vertical σ_1 (Fig. 12a). Stress inversion results for the NW-SE faults indicate a sub-horizontal σ_3 with a N083 azimuth (Fig. 12b).

Basal glide planes deform fine sandstones and marly sandstones of the Kalamavka and Males Formations (Fig. 13). In these planes, E-SE verging sheath folds and injectites are observed through the Ierapetra paleoslope under different blocks. Folds in these deformed levels have sizes that range from tens of centimetres (Fig. 13a) to 4-5 m (Fig. 13b). However, structures generated during block movement are not restricted to the basal intervals. Folding, pinch-and-swell and lateral pinch-out geometries occur in the sandstone beds separating breccia beds, and are often associated with injectites and flame structures at the interface with the overlying coarser material (Fig. 14). These sandstone beds have flat bases parallel to the underlying breccia bed and irregular tops resulting from significant ductile deformation (Fig. 14a, 14b and 14c).

Recumbent folds observed in shear intervals have axial planes with westward dips as low as 10º up to 70º (Fig. 11c and 14a). In contrast, the hinges of sheath folds plunge values between 10º to 40º to the East (Fig. 11d). Such data supports a vergence of the ductile folds concomitant with the general direction of strata remobilisation in basal glide planes. Small-scale injectites sourced from these beds were emplaced within fractures of the overlying beds (Fig. 14b). At outcrops, these types of shear deformation have been observed mostly in the plastic matrix, or at the interface of matrix with mass-transport blocks, but seldom on shear interfaces within individualised blocks- as observed in Ierapetra.

11

6. Discussion

6.1. Multi-scale block deformation

One of the key purposes of comparing MTDs on seismic data to their outcrop equivalents is to assess the similarity of processes occurring at such distinct scales (Bull and Cartwright, 2010; Dykstra et al., 2011; Meckel III, 2011; Ogata et al., 2014; Posamentier and Martinsen, 2011; Posamentier and Walker, 2006). The mass-transport blocks described in this work show a striking uniformity of deformation styles at both seismic and outcrop scales: a) blocks are deformed by two conjugate families of sub-vertical faults and fractures, where one is roughly parallel to the downslope gliding direction; b) paleostress estimates at the time of block movement were also similar for the two case studies (Fig. 7 and 12). There is also a consistent relationship between the shape of the blocks observed at both scales and the strike of the observed fault families.

A first key observation in SE Crete is that closely spaced vertical faults, and associated fractures, occur at scales well below seismic resolution (Fig. 9, 10 and 14). Based on this observation, we suggest closely spaced fractures to occur within seismic-scale blocks in the Espírito Santo Basin (and other continental margins) in association with main faults. In addition, we interpret that fractures might not systematically cross-cut mass-transport blocks along their full height, as lithological contrasts between strata in the blocks are expected to have an important control on fault propagation and growth (Fig. 3a, 9 and 14). In fact, lithological contrasts can hinder fracture propagation into distinct volumes of mass-transport blocks, similarly to the fracture styles observed in SE Crete, which show preferential development in brittle beds (e.g. Fig. 14). A second result in this work is the recognition of bed-parallel shearing in mass-transport blocks during their downslope movement. Bed-parallel shear is documented at both scales of observation (seismic and

outcrop) not only at the base but also at bed-parallel detachment surfaces within blocks (Fig. 3a). The likely occurrence of bed-parallel slip is supported by the shallow SE-striking minimum stress obtained from paleostress calculations (Fig. 7f) and by the identification of low-angle thrust faults and anticlines at seismic scales (Fig. 3a). These are structures that typically occur in association with sub-surface detachment interfaces (Fossen, 2010; Schultz, 2000).

The main contrast between the seismic and outcrop scales concerns the size of the deformation features, with centimetric to metre-size folds occurring at basal intervals of blocks exceeding 20 m in height (Fig. 12, see also Alves and Lourenço, 2010), whereas intra-block shearing is limited to beds with thickness <1m (Fig. 14a, 14b and 14c). The majority of detachment surfaces are better developed along sand-rich beds, indicating a low degree of consolidation in slope strata at the time of block movement. Internal folding is absent in breccia beds, a result of the coarser nature of this sediment and its inability generate ductile structures. We suggest the genesis of bed-parallel structures to relate to limited shearing during the flow of the original carbonate breccias over unconsolidated sandstones. This phenomena was followed by syn-kinematic bed-parallel shear during the downslope movement of blocks. For the latter to occur, strata within discrete blocks had to preserve its ductility to some degree, which allowed for limited flexuring of the outcropping blocks (Alves and Lourenço, 2010) (Fig. 14). Syn-kinematic flexural slip would occur during block movement, with shearing taking place along the sand and marl beds. This assumption is supported by the relatively uniform thickness of the breccias beds, which contrasts with the ductile behaviour of thinned sand beds, recorded as lateral thickness variations and pinch-outs (Fig. 14). Furthermore, the hinge area of such broad flexures shows more closely spaced fractures, with the most prominent cutting across multiple breccias beds (Fig. 14d and 14e).

6.2. 3D flow meshes

On both scales of analysis (seismic and outcrop), faults and fractures generated meshes *sensu* Sibson (1996) that potentially enhance the permeability of mass-transport blocks. Vertical

faults and fractures are potential flow paths extending fully, or partially, through of the blocks (Fig. 15). Wider areas of deformation occur in specific domains where vertical fractures (and chasms) are developed, as suggested by the broad fault zones observed on seismic-scale blocks (Fig. 3 and 4a). However, high densities of shortly-spaced vertical fractures at sub-seismic scales will add to these wider areas of deformation, increasing the permeability of the mass-transport blocks (Fig. 9 and 14).

We interpret, based on the data in this paper, that permeability in discrete blocks is further enhanced at: a) the intersection points of the perpendicular fracture families (Sibson, 1996), and b) at intersections between faults/fractures and bed-parallel shear surfaces (Ligtenberg, 2005; Sibson, 1996), c) in faults and fractures injected by sand sourced from basal glide planes, and d) chasms and other structures indicating important dilation of blocks. At outcrop, not all fractures propagate through the full height of the blocks, often terminating in poorly cemented sand beds (Figs. 9 and 14). These sands, either intact or sheared, will act as permeable bed-parallel conduits connecting near-vertical faults and fractures, especially those of limited vertical extent. Sheared beds presenting soft-sediment deformation features are also relevant as features enhancing vertical permeability by forming entrainments of sandstones within the cemented breccias (Fig 14). Large-scale shearing and associated thrusting, when present within blocks, adds to fluid migration by tilting the original bedding to trigger upward fluid flow along existing permeable strata. Examples of injection structures emplaced in the interface between blocks and fluidized sands have been observed at outcrop as a result of the infill of space created by opening fractures, often extending along the full height of blocks (Ogata et al., 2012). When large chasms are present, they have the potential to allow the injection of fluidized matrix within blocks. This character is relevant for the permeability potential of blocks, especially if the chasms root at sand-rich basal shear levels. Block remobilisation is prone to induce bed-parallel slip and overall fragmentation (Bull et al., 2009; Masson et al., 2006), thus generating tighter meshes towards the central and distal areas of MTDs.

14

7. Conclusions

This paper shows evidence of multi-scale shear within individual mass-transport blocks. The combination of vertical and horizontal compartmentalisation, together with the preserved stratigraphic architecture, originates complex meshes that greatly enhance permeability in discrete blocks. The main results of this work are:

- Mass-transport block deformation styles are identical in the seismic- and outcrop-scale examples studied. Bed-parallel shearing structures and two conjugate families of sub-vertical faults and fractures are observed in the blocks analysed.

- The presence of multi-scale meshes influences the overall permeability potential of blocky MTDs.

- These meshes can create preferential fluid bypass points in mass-transport blocks.

- The concept of the permeable mesh is valid for remnant or rafted blocks in any region of the MTD which maintain their integrity.

- Block remobilisation is prone to induce bed-parallel slip and overall fragmentation, thus generating tighter meshes.

The interpretations in this work have profound implications for the assessment of fluid paths within sedimentary basins, namely those with active venting systems.

References

Alsop, G.I., Marco, S., 2013. Seismogenic slump folds formed by gravity-driven tectonics down a negligible subaqueous slope. Tectonophysics 605, 48-69.

Alves, T.M., 2010. 3D Seismic examples of differential compaction in mass-transport deposits and their effect on post-failure strata. Marine Geology 271, 212-224.

Alves, T.M., 2012. Scale-relationships and geometry of normal faults reactivated during gravitational gliding of Albian rafts (Espírito Santo Basin, SE Brazil). Earth and Planetary Science Letters 331–332, 80-96.

Alves, T.M., Kurtev, K., Moore, G.F., Strasser, M., 2014. Assessing the internal character, reservoir potential, and seal competence of mass-transport deposits using seismic texture: A geophysical and petrophysical approach. AAPG Bulletin 98, 793-824.

Alves, T.M., Lourenço, S.D.N., 2010. Geomorphologic features related to gravitational collapse: Submarine landsliding to lateral spreading on a Late Miocene-Quaternary slope (SE Crete, eastern Mediterranean). Geomorphology 123, 13-33.

Barker, P.F., Buffler, R.T., Gambôa, L.A., 1983. A seismic reflection study of the Rio Grande Rise, in: Barker, P.F., Carlson, R.L., Hohnson, D.A. (Eds.), Initial Reports of the Deep Sea Drilling Program, Washington, D.C., Government Printing Office, pp. 953-976.

Beaubouef, R.T., Abreu, V., 2010. MTCs of the Brazos-Trinity Slope System; Thoughts on the Sequence Stratigraphy of MTCs and Their Possible Roles in Shaping Hydrocarbon Traps, in: Mosher, D.C., Shipp, R.C., Moscardelli, L., Chaytor, J.D., Baxter, C.D.P., Lee, H.J., Urgeles, R. (Eds.), Submarine Mass Movements and Their Consequences. Springer, pp. 475-490.

Brown, A.R., 2004. Interpretation of Three-Dimensional Seismic Data, sixth ed. American Association of Petroleum Geologists, Tulsa.

Bull, S., Cartwright, J., 2010. Small-scale insights into seismic-scale slumps: A comparison of slump features from the waitemata basin, New Zealand, and the Møre Basin, Off-Shore Norway, Submarine Mass Movements and Their Consequences - 4th International Symposium, pp. 257-266.

Bull, S., Cartwright, J., Huuse, M., 2009. A review of kinematic indicators from mass-transport complexes using 3D seismic data. Marine and Petroleum Geology 26, 1132-1151.

Callot, P., Odonne, F., Sempere, T., 2008. Liquification and soft-sediment deformation in a limestone megabreccia: The Ayabacas giant collapse, Cretaceous, southern Peru. Sedimentary Geology 212, 49-69.

Davison, I., 2007. Geology and tectonics of the South Atlantic Brazilian salt basins, in: Ries, A.C., Butler, R.W.H., Graham, R.H. (Eds.), Deformation of the Continental Crust: The Legacy of Mike Coward. Geological Society London, Special Publications 272, pp. 345-359.

De Blasio, F.V., Engvik, L.E., Elverhøi, A., 2006. Sliding of outrunner blocks from submarine landslides. Geophysical Research Letters 33.

Demercian, S., Szatmari, P., Cobbold, P.R., 1993. Style and pattern of salt diapirs due to thin-skinned gravitational gliding, Campos and Santos basins, offshore Brazil. Tectonophysics 228, 393-433.

Dunlap, D.B., Wood, L.J., Weisenberger, C., Jabour, H., 2010. Seismic geomorphology of offshore Morocco's east margin, Safi Haute Mer area. AAPG Bulletin 94, 615-642.

Dykstra, M., Garyfalou, K., Kertznus, V., Kneller, B., Milana, J.P., Molinaro, M., Szuman, M., Thompson, P., 2011. Mass-transport deposits: combining outcrop studies and seismic forward modeling to understand lithofacies distributions, deformation, and their seismic stratigraphic expression, in: Shipp, C., Weimer, P., Posamentier, H. (Eds.), Mass-transport deposits in deepwater settings. SEPM Special Publication 96, pp. 293-310.

Fiduk, J.C., Brush, E.R., Anderson, L.E., Gibbs, P.B., Rowan, M.G., 2004. Salt deformation, magmatism, and hydrocarbon prospectivity in the Espirito Santo Basin, offshore Brazil, in: Post, P.J., Olson, D.L., Lyons, K.T., Palmes, S.L., Harison, P.F., Rosen, N.C. (Eds.), Salt-sediment interactions and hydrocarbon prospectivity: Concepts, applications, and case studies for the 21st century. GCSSEPM 24th Annual Research Conference, pp. 370-392.

Fossen, H., 2010. Structural Geology. Cambridge University Press.

França, R.L., Del Rey, A.C., Tagliari, C.V., Brandão, J.R., Fontanelli, P.R., 2007. Bacia de Espírito Santo. Boletim de Geociências da Petrobras 15, 501-509.

Frey-Martinez, J., Cartwright, J., Hall, B., 2005. 3D seismic interpretation of slump complexes: examples from the continental margin of Israel. Basin Research 17, 83-108.

Frey-Martínez, J., Cartwright, J., James, D., 2006. Frontally confined versus frontally emergent submarine landslides: A 3D seismic characterisation. Marine and Petroleum Geology 23, 585-604.

Gamboa, D., Alves, T., Cartwright, J., 2011. Distribution and characterization of failed (mega) blocks along salt ridges, southeast Brazil: Implications for vertical fluid flow on continental margins. Journal of Geophysical Research 116, B08103.

Gamboa, D., Alves, T., Cartwright, J., Terrinha, P., 2010. MTD distribution on a 'passive' continental margin: The Espírito Santo Basin (SE Brazil) during the Palaeogene. Marine and Petroleum Geology 27, 1311-1324.

Gamboa, D., Alves, T.M., Cartwright, J., 2012. Seismic-Scale Rafted and Remnant Blocks over Salt Ridges in the Espírito Santo Basin, Brazil, in: Yamada, Y., Kawamura, K., Ikehara, K., Ogawa, Y., Urgeles, R., Mosher, D.C., Chaytor, J.D., Strasser, M. (Eds.), Submarine Mass Movements and Their Consequences. Springer, pp. 629-638.

Gee, M.J.R., Gawthorpe, R.L., Friedmann, J.S., 2005. Giant striations at the base of a submarine landslide. Marine Geology 214, 287-294.

Hampton, M.A., Lee, H.J., Locat, J., 1996. Submarine Landslides. Review of Geophysics 34, 33-59.

Ilstad, T., De Blasio, F.V., Elverhøi, A., Harbitz, C.B., Engvik, L., Longva, O., Marr, J.G., 2004. On the frontal dynamics and morphology of submarine debris flows. Marine Geology 213, 481-497.

Jackson, C.A.L., 2011. Three-dimensional seismic analysis of megaclast deformation within a mass transport deposit; implications for debris flow kinematics. Geology 39, 203-206.

Kvalstad, T.J., Andresen, L., Forsberg, C.F., Berg, K., Bryn, P., Wangen, M., 2005. The Storegga slide: evaluation of triggering sources and slide mechanics. Marine and Petroleum Geology 22, 245-256.

Ligtenberg, J.H., 2005. Detection of fluid migration pathways in seismic data: implications for fault seal analysis. Basin Research 17, 141-153.

Lisle, R.J., Srivastava, D.C., 2004. Test of the frictional reactivation theory for faults and validity of fault-slip analysis. Geology 32, 569-572.

Lucente, C.C., Pini, G.A., 2008. Basin-wide mass-wasting complexes as markers of the Oligo-Miocene foredeep-accretionary wedge evolution in the Northern Apennines, Italy. Basin Research 20, 49-71.

Masson, D.G., Harbitz, C.B., Wynn, R.B., Pedersen, G., Løvholt, F., 2006. Submarine landslides: Processes, triggers and hazard prediction. Philosophical Transactions: Mathematical, Physical and Engineering Sciences (Series A) 364, 2009-2039.

McFarland, J.M., Morris, A.P., Ferrill, D.A., 2012. Stress inversion using slip tendency. Computers & Geosciences 41, 40-46.

Meckel III, L.D., 2011. Reservoir characteristics and classification of sand-prone submarine mass-transport deposits, in: Shipp, C., Weimer, P., Posamentier, H. (Eds.), Mass-transport deposits in deepwater settings. SEPM Special Publication 96, pp. 423-450.

Mohriak, W.U., 2003. Bacias sedimentares da margem continental Brasileira, in: Bizzi, L.A., Schobbenhaus, C., Vidotti, R.M., Goncalves, J.H. (Eds.), Geologia, Tectonica e Recursos Minerais do Brasil. CPRM, Brasilia, pp. 87-165.

Mohriak, W.U., 2005. Interpretação geológica e geofísica da Bacia do Espírito Santo e da região de Abrolhos: Petrografia, datação radiométrica e visualização sísmica das rochas vulcânicas. Boletim de Geociencias da Petrobras 14, 133-142.

Mohriak, W.U., Rabelo, J.H.L., De Matos, R.D., De Barros, M.C., 1995. Deep seismic reflection profiling of sedimentary basins offshore Brazil: geological objectives and preliminary results in the Sergipe Basin. Journal of Geodynamics 20, 515-539.

Moreira, J.L.P., Carminatti, M., 2004. Sistemas deposicionais de talude e de bacia no Eoceno da Bacia de Santos. Boletim de Geociencias da Petrobras 12, 73-87.

Morris, A., Ferrill, D.A., Henderson, D.B., 1996. Slip-tendency analysis and fault reactivation. Geology 24, 275-278.

Mulder, T., Cochonat, P., 1996. Classification of offshore mass movements. Journal of Sedimentary Research 66, 43-57.

Nemec, W., 1990. Aspects of sediment movement on steep delta slopes.

Ogata, K., Mountjoy, J.J., Pini, G.A., Festa, A., Tinterri, R., 2014. Shear zone liquefaction in mass transport deposit emplacement: A multi-scale integration of seismic reflection and outcrop data. Marine Geology 356, 50-64.

Ogata, K., Mutti, E., Pini, G.A., Tinterri, R., 2012. Mass transport-related stratal disruption within sedimentary mélanges: Examples from the northern Apennines (Italy) and south-central Pyrenees (Spain). Tectonophysics 568–569, 185-199.

Ogiesoba, O., Hammes, U., 2012. Seismic interpretation of mass-transport deposits within the upper Oligocene Frio Formation, south Texas Gulf Coast. AAPG bulletin 96, 845-868.

Ojeda, H.A.O., 1982. Structural framework, stratigraphy, and evolution of Brazilian marginal basins. AAPG Bulletin 66, 732-749.

Omosanya, K.d.O., Alves, T.M., 2013a. Ramps and flats of mass-transport deposits (MTDs) as markers of seafloor strain on the flanks of rising diapirs (Espírito Santo Basin, SE Brazil). Marine Geology 340, 82-97.

Omosanya, K.d.O., Alves, T.M., 2014. Mass-transport deposits controlling fault propagation, reactivation and structural decoupling on continental margins (Espírito Santo Basin, SE Brazil). Tectonophysics 628, 158-171.

Omosanya, K.O., Alves, T.M., 2013b. A 3-dimensional seismic method to assess the provenance of Mass-Transport Deposits (MTDs) on salt-rich continental slopes (Espírito Santo Basin, SE Brazil). Marine and Petroleum Geology 44, 223-239.

Posamentier, H., 2004. Stratigraphy and geomorphology of deep-water mass transport complexes based on 3D seismic data, Offshore Technology Conference, Houston, TX.

Posamentier, H., Martinsen, O.J., 2011. The character and genesis of submarine mass-transport deposits: insights from outcrop and 3D seismic data, in: Shipp, C., Weimer, P., Posamentier, H. (Eds.), Mass-transport deposits in deepwater settings. SEPM Special Publication 96, pp. 7-38.

Posamentier, H., Walker, R.G., 2006. Deep water turbidites and submarine fans, in: Posamentier, H., Walker, R.G. (Eds.), Facies Models Revisited - SEPM Special Publication. SEPM (Society for Sedimentary Geology), Tulsa, Oklahoma, U.S.A., pp. 397-520.

Postma, G., Drinia, H., 1993. Architecture and sedimentary facies evolution of a marine, expanding outer-arc half-graben (Crete, late Miocene). Basin research 5, 103-124.

Schultz, R.A., 2000. Localization of bedding plane slip and backthrust faults above blind thrust faults: Keys to wrinkle ridge structure. Journal of Geophysical Research: Planets (1991–2012) 105, 12035-12052.

Sibson, R.H., 1996. Structural permeability of fluid-driven fault-fracture meshes. Journal of Structural Geology 18, 1031-1042.

Solheim, A., Berg, K., Forsberg, C.F., Bryn, P., 2005. The Storegga Slide complex: repetitive large scale sliding with similar cause and development. Marine and Petroleum Geology 22, 97-107.

Weimer, P., Shipp, C., 2004. Mass transport complex: musing on the past uses and suggestions for future directions, Offshore Technology Conference, Houston, Texas.

Figure captions

Fig. 1. Locations maps of the study areas in the **a**) Espírito Santo Basin and **b**) Ierapetra Basin. Modified after Alves and Lourenço (2010) and Gamboa et al. (2011).

Fig. 2. a) Seafloor image of the study area of the Espírito Santo Basin showing modern SE-directed turbidite systems. **b**) Seismic profile depicting the studied MTD in the Espírito Santo Basin. The interpreted Miocene MTD includes multiple mass-transport blocks (B) that cause marked irregularities in the Top horizon. **c**) Seismic variance map parallel to the Base MTD horizon. Larger blocks are located on the proximal region of the MTD, with progressively smaller blocks being observed eastwards due to fragmentation. Fracturing is observed in numerous blocks in proximal and central areas of the MTD. **d**) Geological map of the studied paleoslope of the Ierapetra Basin. Remobilised blocks from the Prina Series are present over the Kalamavka and Males Formations. The rose diagram shows the principal directions of transport of the blocks.

Fig. 3. Seismic sections depicting Block A. **a**) Seismic profile parallel to the MTD direction of movement, showing a high-amplitude lower section (LS) and a moderate amplitude upper section (US) separated by horizon H1. Two thrust faults (Tf) and anticlines (Ta) are present in the upper section (US). Normal faults (f) are more numerous in the upper section comparatively to the lower section. A frontal anticline (Fa) is observed in the lower section. **b**) Profile perpendicular to the MTD direction of movement. Extensional faults (f) are observed both in the lower and upper

sections along this orientation. Two main fault-bounded chasms (Ch) developed due to extension. The large chasm-bounding faults extend along the full block height, connecting the base and top levels. dm- disaggregated matrix.

Fig. 4. a) Variance slice across Block A depicting the sub-perpendicular fault families (f), the thrust faults (Tf) and dilational chasms (Ch). **b**) RMS amplitude map of a 40 ms time-window centred in H1. High-amplitude patches underlie the areas where thrust anticlines are present, and delimited by the thrust faults (Tf) at the front. The high-amplitudes are interpreted as intervals prone to ductile shearing.

Fig. 5. Stereonet and orientation rose diagrams of the faults mapped in the block A. **a**) Includes all the faults in the block, **b**) Faults mapped in the lower section (LS), **c**) All faults in the upper section (US), **d**) Chasm faults and **e**) Thrust faults.

Fig. 6. 3D view of the interconnected mesh created by faults and horizons mapped in Block A. Coloured surfaces represent changes in dip along the fault planes. Note that the shallower dips are observed in the thrusts faults (Tf). The large faults bounding the chasms (Ch 1 and 2) propagate in the full height of the block. The shading in H1 and basal glide plane horizons highlights the curvature on these two sub-horizontal surfaces.

Fig. 7. Diagrams representing the paleostress conditions obtained from the stress inversion of the faults in Block A. **a**) Inversion of all mapped faults indicate a SE-striking minimum stress (σ_3). **b**) Inversion of the lower section (LS) faults show SE-striking extension. **c**) and **d**) Inversion of the upper section (US) sub-perpendicular fault families. Paleostress calculations show two main stress fields controlling fault extension in the upper section with conjugate ESE- and N-striking σ_3 tensors. **e**) Inversion of the chasm faults show a NE-oriented extension. **f**) Stress inversion of the

thrust faults in the US, indicating a low-angle, SE-directed maximum compression tensor (σ_1), parallel to the direction of movement of Block A.

Fig. 8. 3D visualisation of the slip tendency of faults and interpreted shear surfaces under distinct paleostresses. **a**) Low to moderate slip tendencies occur under paleostress conditions obtained from stress inversion of all faults (see Fig. 7a). The lower slip is observed in the sub-horizontal H1 and basal glide plane. **b**) Moderate to high slip tendencies occur under paleostress conditions computed from thrust faults. This allows high slip along the interpreted shear horizon H1. High slip tendencies are also observed in parts of extensional faults.

Fig. 9. Block in the Males Formation showing fractured cemented sandstones (sst) detaching along gravel beds (grv). The latter beds have lower degrees of cementation and irregular thickness. The fractures (f) propagating in the sandstone beds often terminate at the interface with the gravel beds.

Fig. 10. Panoramic view of mass-transport blocks in the Ierapetra Basin. Outcropping blocks show vertical fracture families (f) arranged in two sub-perpendicular families. Chasms (Ch) also develop within blocks, associated with the fracturing during downslope movement. The flanks of the blocks tend to be related to the orientation of the fractures.

Fig. 11. Stereonet and rose diagrams of fractures mapped in outcropping blocks, SE Crete. **a**) Fractures in Males Formation blocks. **b**) Fractures in the Prina blocks. **c**) Axial planes of recumbent folds in sheared strata. **d**) Hinge lineations of sheath folds.

Fig. 12. Diagrams representing the paleostress conditions obtained from the inversion of faults and fractures in Prina Series blocks. The tensors of minimum stress (σ_3) show a sub-perpendicular orientation towards the ESE sector, concomitant with the direction of movement of the blocks.

Fig. 13. Examples of sheared intervals of basal glide planes. **a**) Centimetre-scale folds in fine-grained sandstone beds. There is a layer-bound distinction in fold size, with larger fold occurring in the upper level. **b**) Metre-scale folds in heterolithic beds composed of sandstones and pebble beds, part of the basal glide plane of a mass-transport block.

Fig. 14. Detail of deformation structures of outcropping blocks. **a**) Entrainment of folded sand beds in breccia beds deformed by ductile shearing. b**)** Ductile deformation of sandstone beds, with load casts and upward injection features associated with fractures in the breccia beds. **c**) Folding and entrainment of sandstone in breccias resulting from bed-parallel shearing. **d** and **e**) Examples of fracturing and bending along the width and length of the blocks. sst- sandstone; brc – breccia; f-faults/fractures; Ch- chasms.

Fig. 15. Schematic diagram of fault and fracture meshes within mass-transport blocks. Fluids can propagate vertically through the block along fault and fractures, and horizontally along sheared beds. Fluid percolation is more significant at intersection points of the sub-perpendicular faults and fracture families with sheared beds.

Figure 1

Figure 2

Figure 3

28

Figure 4

A All faults — n=38

B Faults in lower section — n=3

C Faults in upper section — n=14

D Faults in chasms — n=8

E Thrust faults — n=6
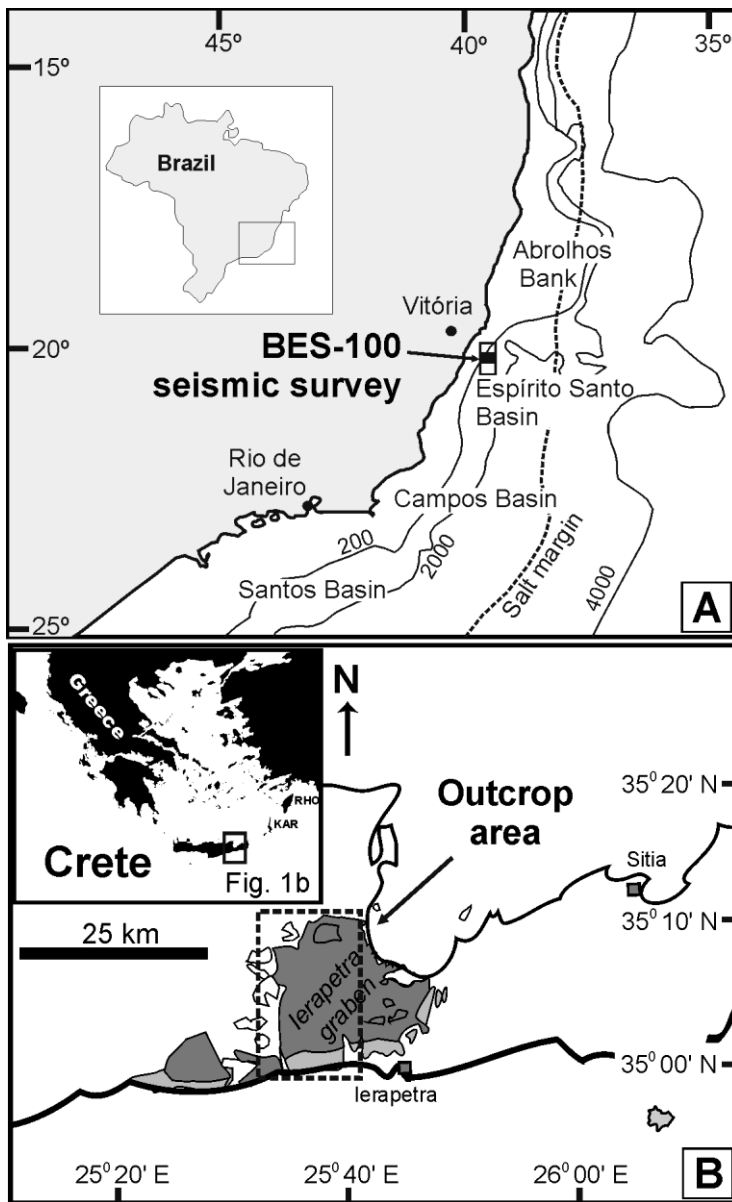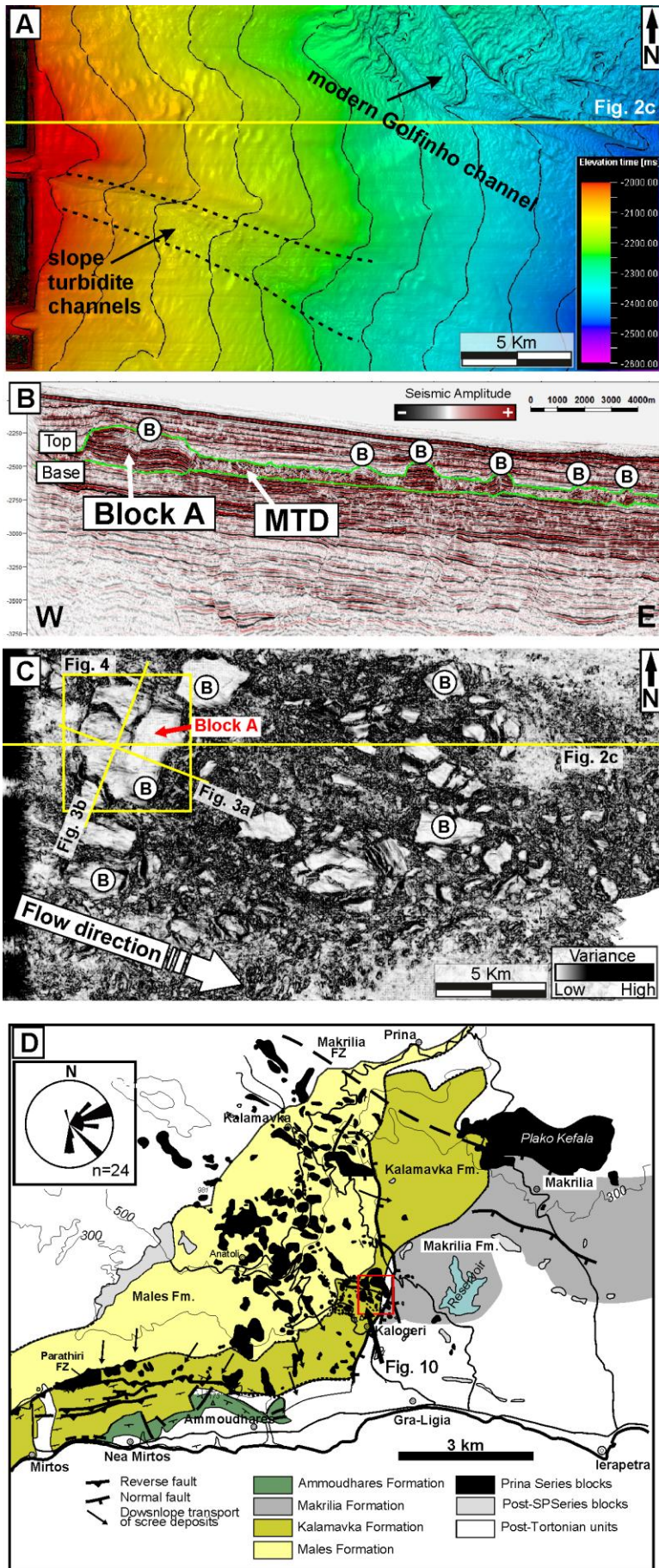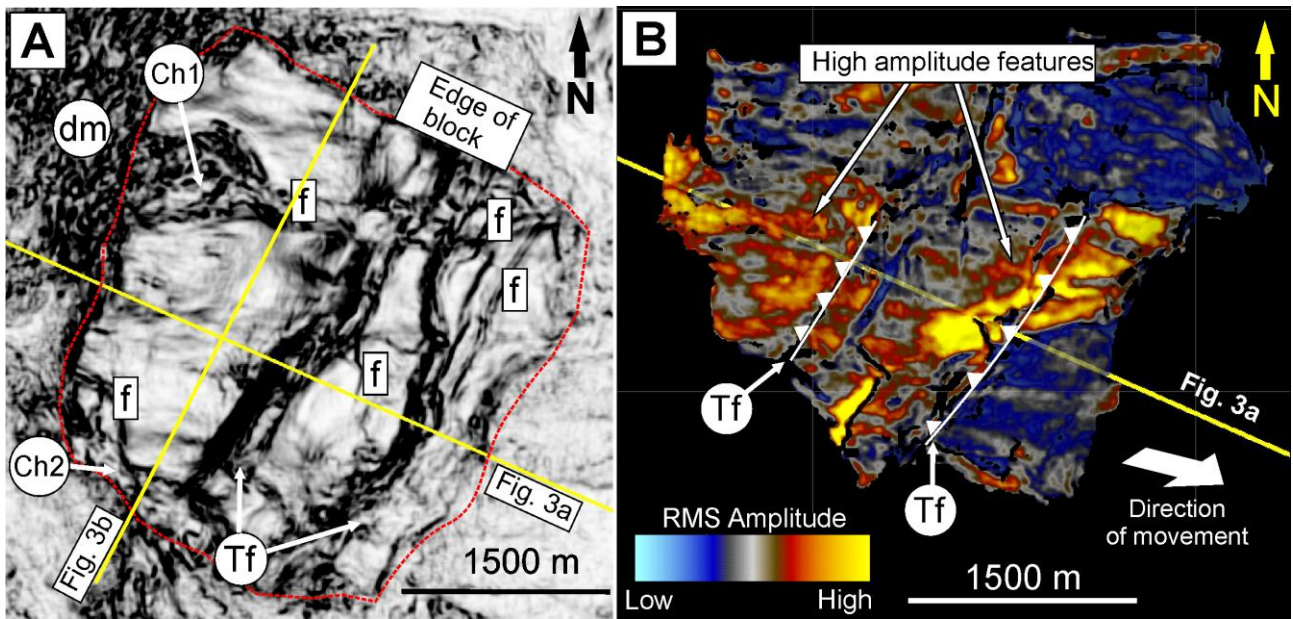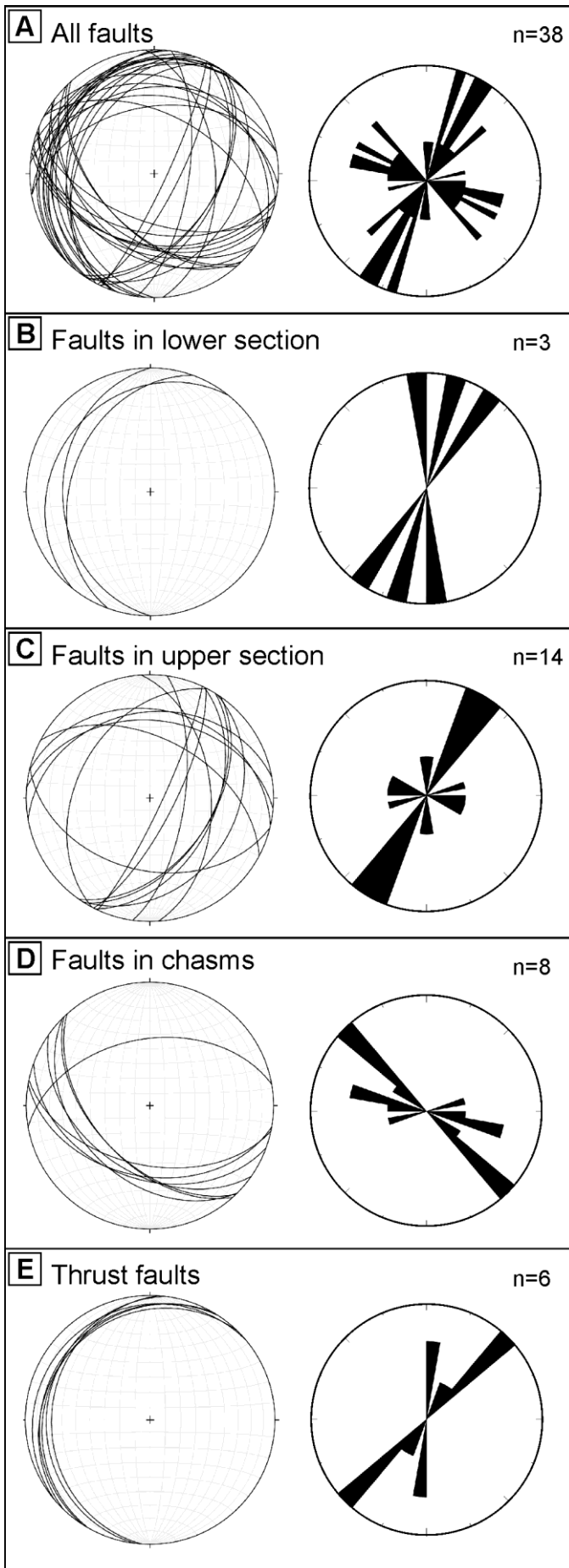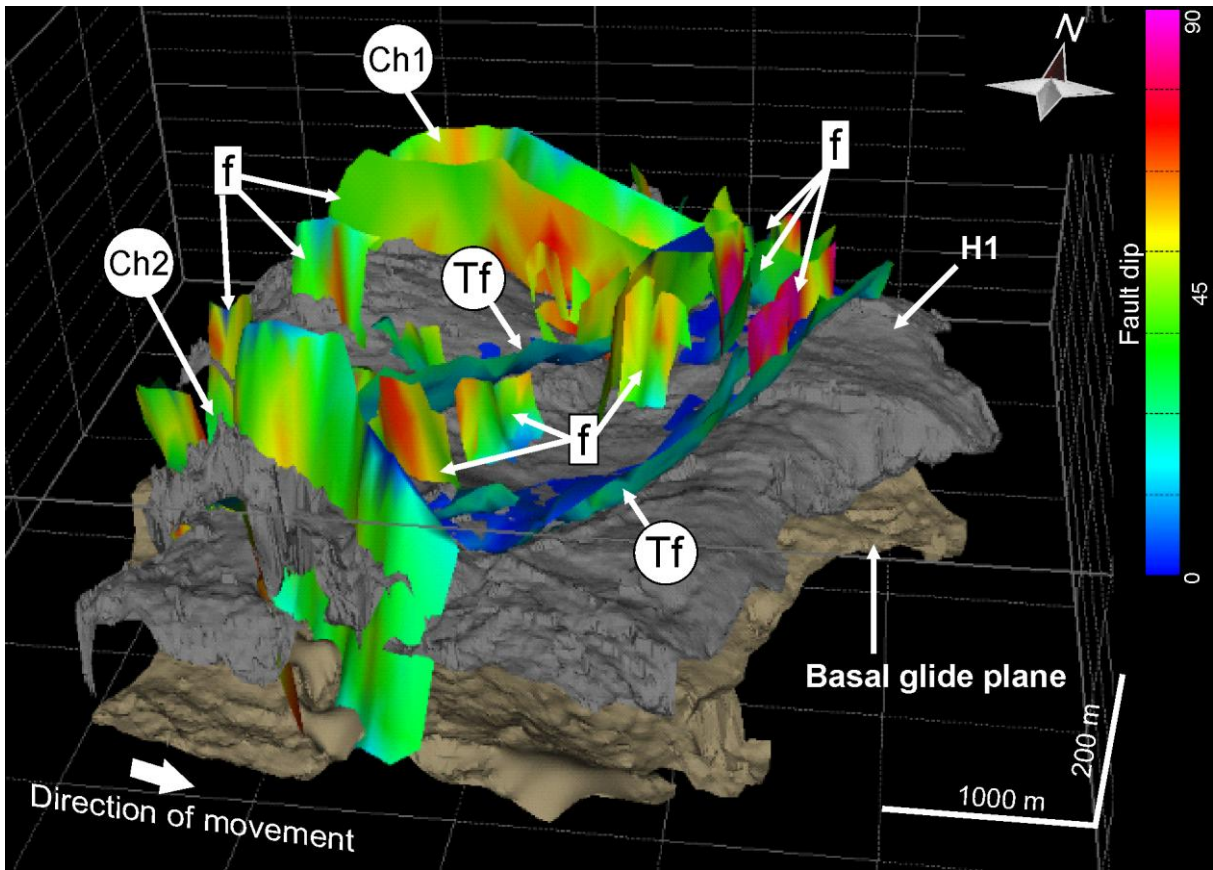
Figure 5

Figure 6

Stress inversion diagrams for faults in Block A:

Figure 7

Figure 8

33
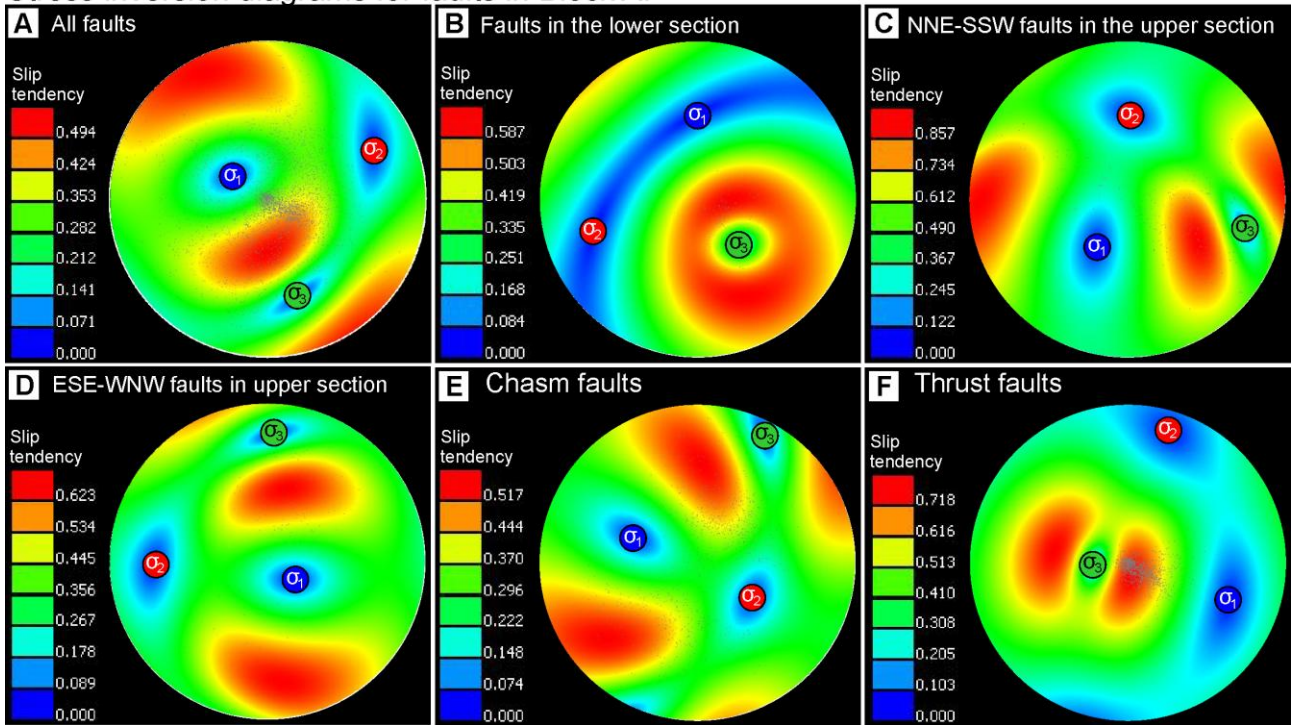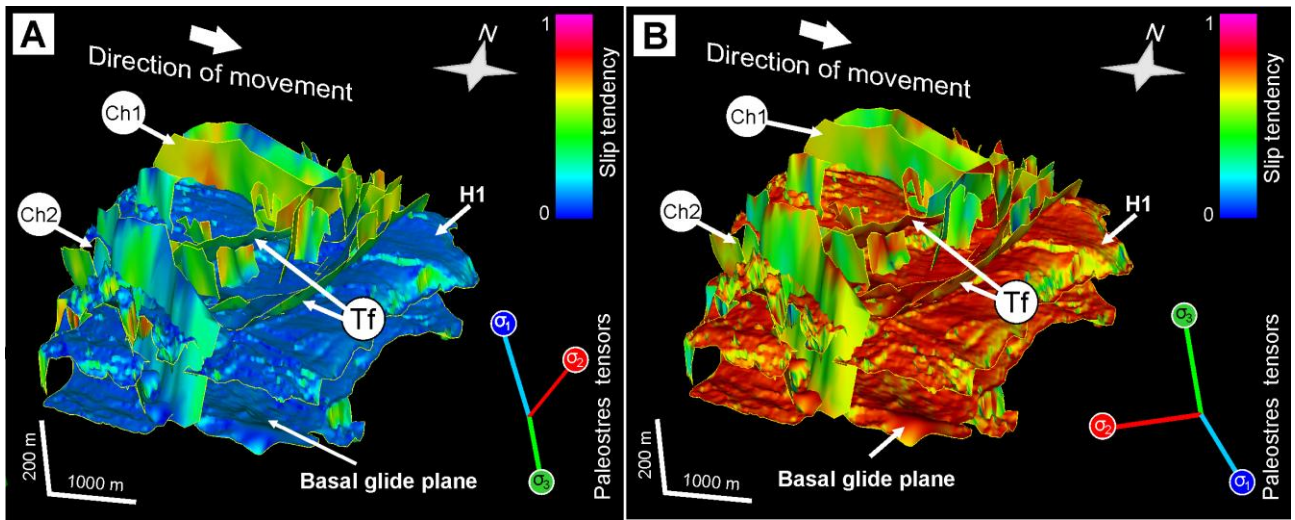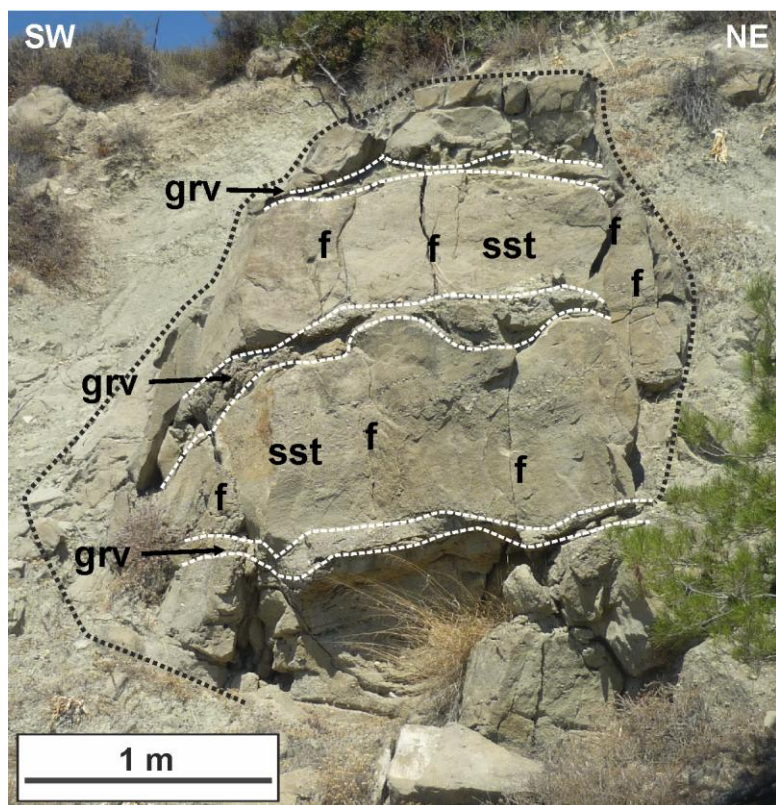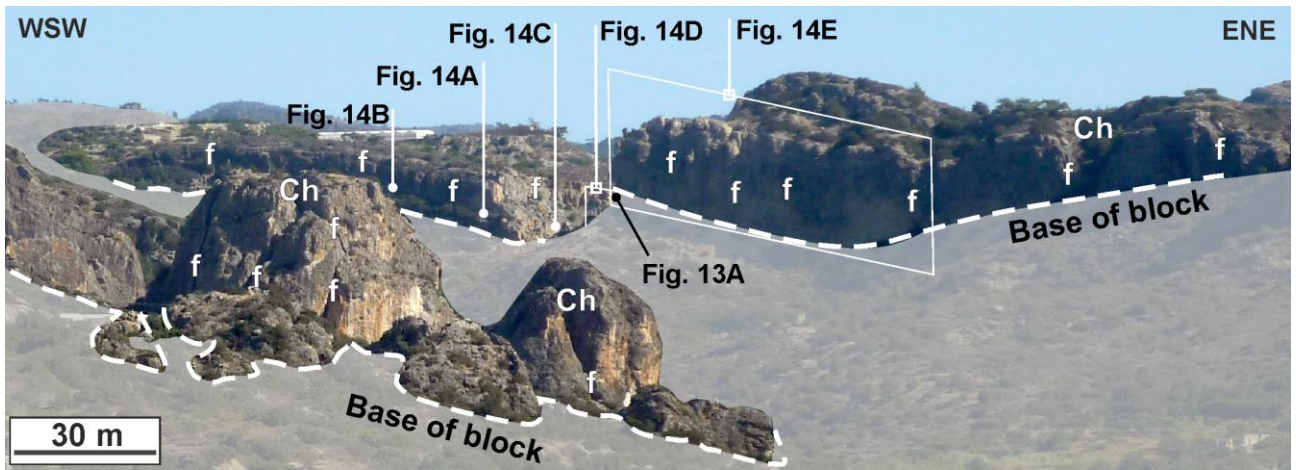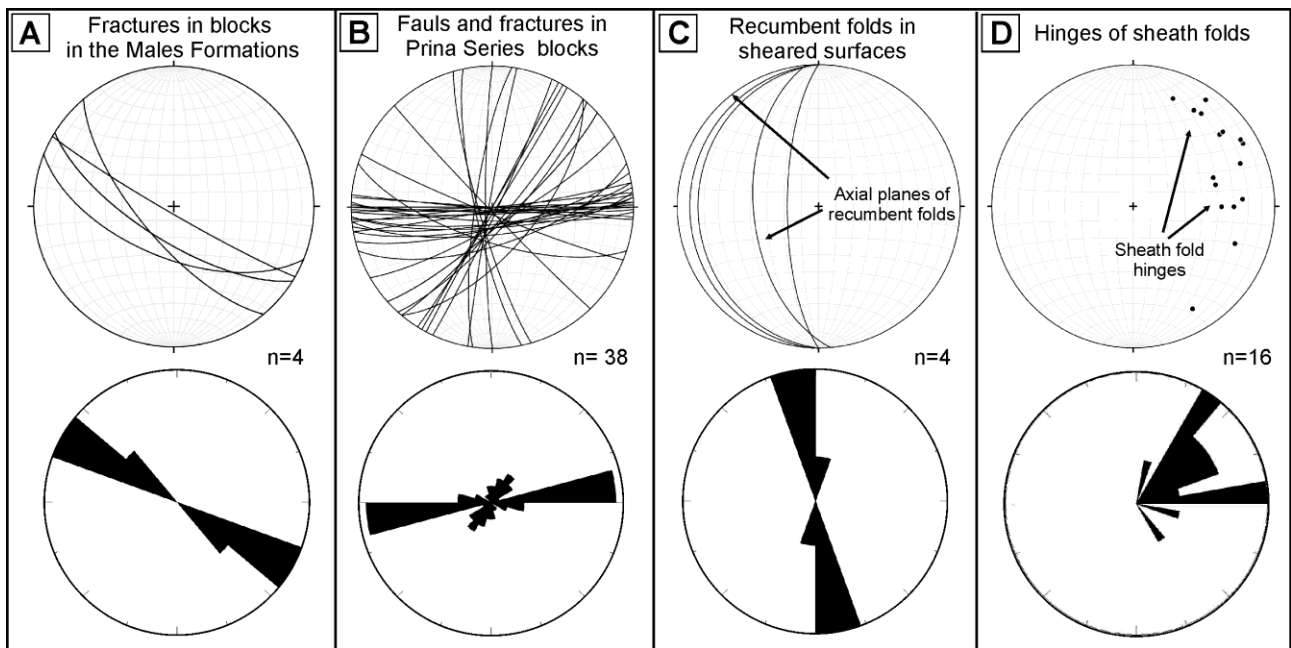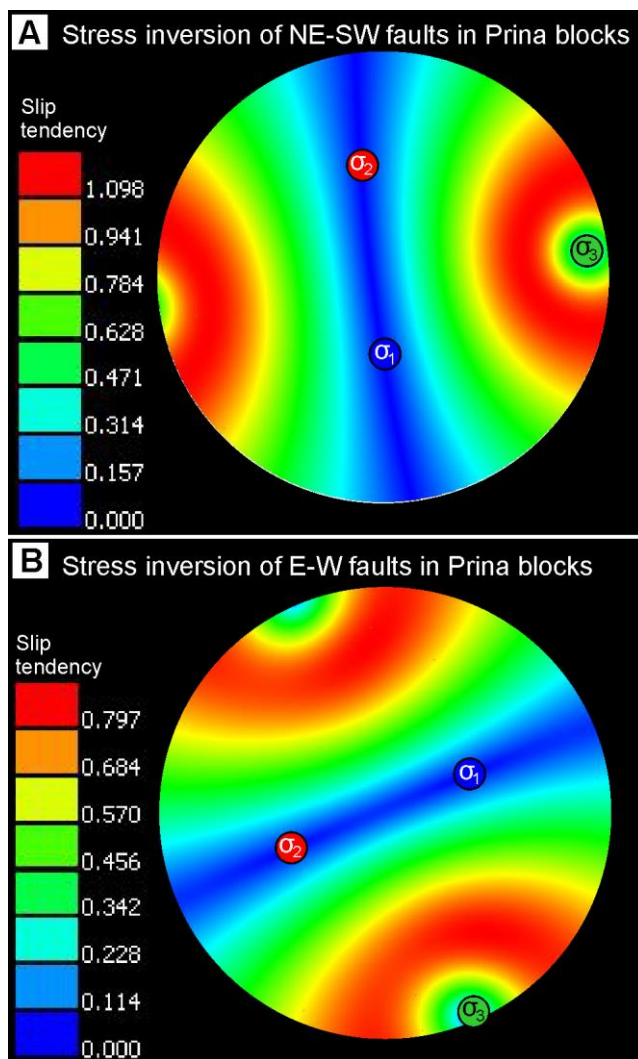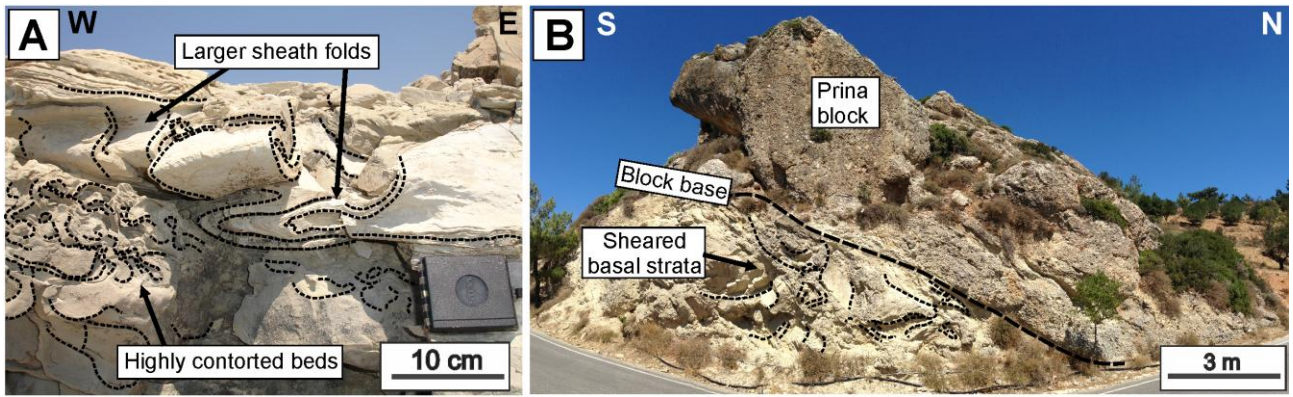
Figure 9
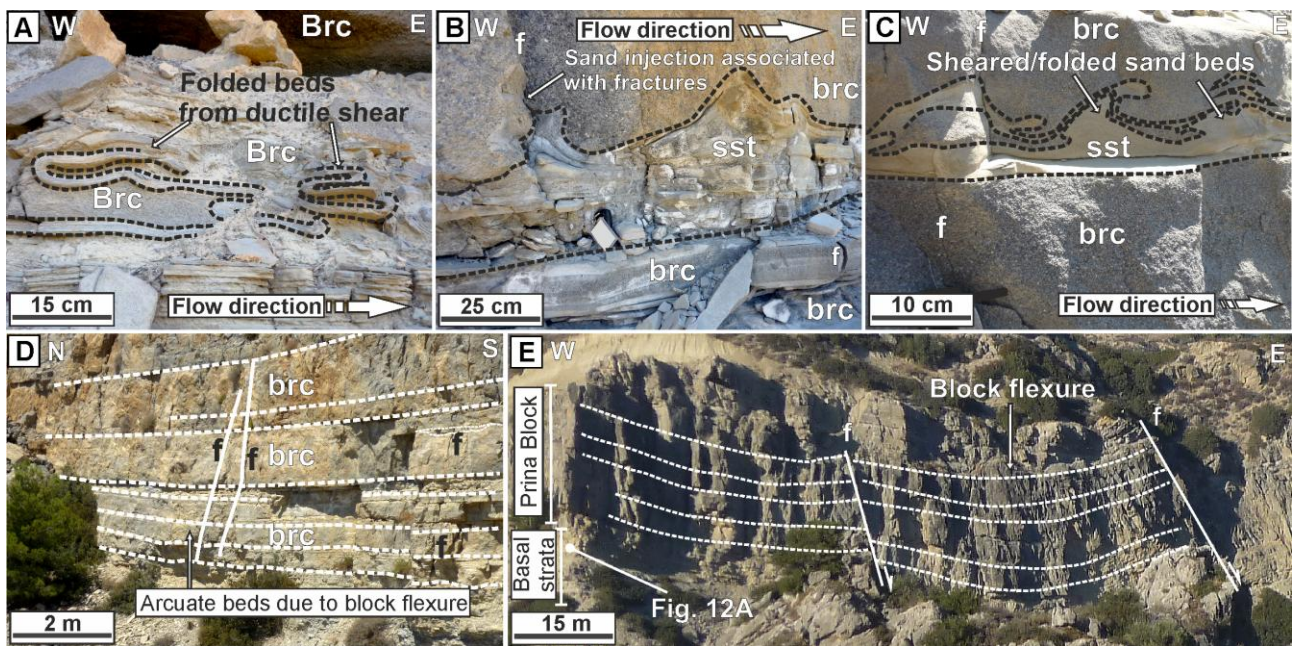
Figure 10

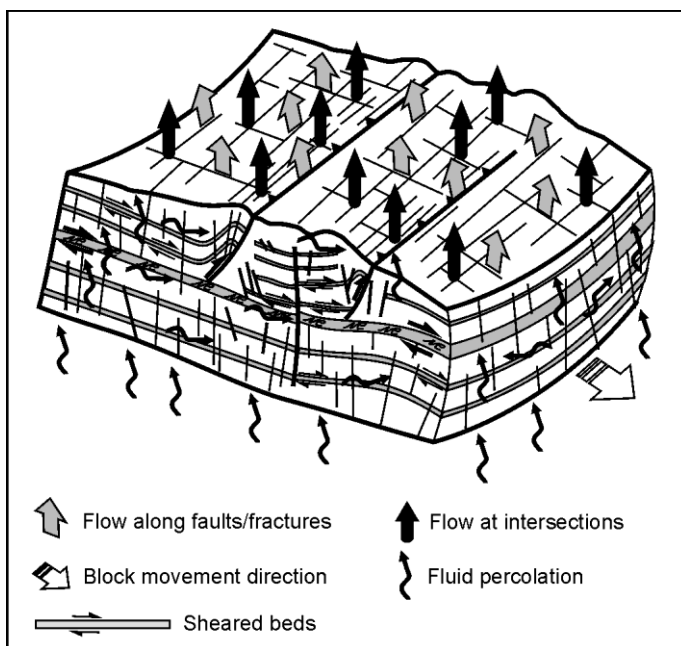Figure 11

Figure 12

Figure 13

Figure 14

Figure 15

Highlights

- Shear structures are identified in seismic-scale mass-transport blocks
- Shear structures in outcrops blocks develop along ductile beds.
- Sub-perpendicular faults and fractures are identified in mass-transport blocks
- Deformation meshes in blocks formed intersecting fractures and shear structures
- Multi-scale deformation meshes increase permeability of mass-transport blocks